# High-Performance Field Effect Transistors from Solution Processed Carbon Nanotubes

**Huiliang Wang,[†] Jun Luo,[†] Alex Robertson,[†] Yasuhiro Ito,[†] Wenjing Yan,[†] Volker Lang,[†] Mujtaba Zaka,[†] Franziska Schäffel,[†] Mark H. Rümmeli,[‡,§] G. Andrew D. Briggs,[†] and Jamie H. Warner[†,*]**

[†]Department of Materials, University of Oxford, Parks Road, Oxford, OX1 3PH, United Kingdom, [‡]IFW Dresden, P.O. Box 270116, D-01171 Dresden, Germany, and [§]Technische Universität Dresden, Dresden, D-01062, Germany

**ABSTRACT** Nanoelectronic field effect transistors (FETs) are produced using solution processed individual carbon nanotubes (CNTs), synthesized by both arc discharge and laser ablation methods. We show that the performance of solution processed FETs approaches that of CVD-grown FETs if the nanotubes have minimal lattice defects and are free from surface contamination. This is achieved by treating the nanotubes to a high-temperature vacuum annealing process and using 1,2-dichloroethane for dispersion. We present CNT FETs with mobilities of up to 3546 $cm^2/(V\ s)$, transconductance of 4.22 μS, on-state conductance of 9.35 μS and on/off ratios as high as $10^6$. High-resolution transmission electron microscopy is used to examine the presence of catalyst particles and amorphous carbon on the surface and Raman spectroscopy is used to examine the lattice defects, both of which lead to reduced device performance.

**KEYWORDS:** carbon nanotube · solution processed · high-performance · TEM · transistor

Carbon nanotubes (CNTs) are potential materials for future nanoelectronics owing to their exceptional electrical properties and one-dimensional structure. They have been used to make field-effect transistors,[1,2] chemical sensors,[3] memory devices,[4] and elements in transparent electronics.[5] Currently, the highest performance CNT devices are fabricated from CNTs which were grown by chemical vapor deposition (CVD). These devices demonstrate a charge carrier mobility (μ) of up to 100000 $cm^2/(V\ s)$, where the highest value is found from a CNT device with an extremely long channel,[6] and a conductance close to quantum conductance ($G = 4e^2/h = 155$ μS).[7] The highest on/off ratio reported recently is $10^7$.[8] However, the high-growth temperature during the CVD process can damage the electrodes, substrates, or other components of complementary metal-oxide-semiconductor (CMOS) technology.

Devices of solution processed CNTs can be made at room temperature and are compatible with CMOS technology and flexible electronics.[9] Solution processed CNTs can also be separated into their semiconducting and metallic counterparts by density gradient ultracentrifugation[10] or substrate surface modification.[11] Dielectrophoresis (DEP) has been used to fabricate a large number of CNT transistors simultaneously.[12] However, the device performance of solution-processed CNT devices is generally poorer than that of CVD-grown ones, possibly due to defects in the CNTs induced by intense acid treatment at the purification stage, surface contamination, and subsequent aggressive sonication at the dispersion stage.[13] Solution processed devices fabricated by Stokes *et al.* using DEP have mobilities of 1380 $cm^2/(V\ s)$ and the on-state conductances of 6 μS,[12] which are an order of magnitude improvement over previous solution-processed devices produced by DEP ($G_{on} = 1.0$ μS),[14] by drop casting ($\mu_{max} = 60\ cm^2/(V\ s)$)[15] and by dip-pen lithography ($\mu = 67\ cm^2/(V\ s)$).[16] Recently a high-performing CNT device produced by spin coating also showed a conductance of 2.5 μS, transconductance of 1.27 μS, and an on/off ratio of $10^6$.[17]

The improvements to CNT device performance have been mainly focused on the design of device[17] or the materials used for electrodes[7] and dielectrics[18] rather than the control of the structures and environments of the CNTs. Here, we show that solution-processed CNT devices can have large mobilities and on/off ratios, similar to CVD-grown CNTs. We use transmission electron microscopy (HRTEM) and Raman spectroscopy to characterize the structural properties and correlate this to device performance.

## RESULT AND DISCUSSION

More than 50 devices were produced from the FHP CNTs and the PtRhRe CNTs

*Address correspondence to Jamie.warner@materials.ox.ac.uk.

Received for review August 18, 2010 and accepted October 06, 2010.

**Published online October 19, 2010.** 10.1021/nn1020743

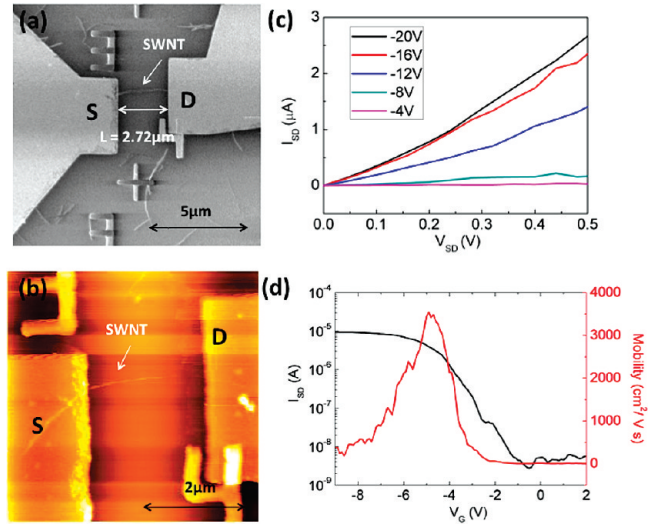


**Figure 1. Characterization of a FHP CNT device (device 1). (a) SEM image of device 1 showing its channel length (*L*) to be 2.72 μm, where "S" and "D" denote source and drain, respectively. (b) AFM image of the device. (c) Current−voltage (*IV*) characteristics of the device, where $I_{SD}$ and $V_{SD}$ denote the current and the voltage between the source and drain, respectively. (d) Transfer characteristics of device 1 showing dependences of $I_{SD}$ and the mobility on the gate voltage ($V_G$), when $V_{SD}$ = 1 V.**

using EBL with a yield over 90%, demonstrating that a reliable way of fabrication of CNT devices has been established. We found that eight of the FHP devices displayed semiconducting behavior, while the rest were metallic. The large portion of metallic FHP devices is attributed to the device containing single metallic CNTs or small bundles containing metallic CNTs. For the PtRhRe CNTs, we found the majority exhibited metallic behavior and only two showed semiconducting properties. We believe that this is due to the doping of the SWNT by the residual metal catalyst and its interaction with the host solvent. In this report the focus on the electrical properties of devices that exhibit semiconducting behavior and have potential for field effect transistors. A high-performing field effect transistor device (device 1) made from FHP CNTs is shown in Figure 1. The channel length of the device was measured to be 2.72 μm from the SEM image in Figure 1a, and the diameter of the CNT was measured to be 1.5 nm from the AFM image in Figure 1b.

The transfer characteristics of the device are illustrated in Figure 1c,d. The CNT conducts well at negative $V_G$ but becomes almost insulating at high positive $V_G$, indicating that the CNT is p-type semiconducting. The peak conductance and the peak transconductance are calculated to be 9.35 μS and 4.22 μS, respectively, where the transconductance ($g_m$) is given by

$$g_m = dI_{SD}/dV_G \quad (1)$$

The mobility shown in Figure 1d is determined using the equation[16]

$$\mu = \frac{L}{V_{SD}C_t}\frac{dI_{SD}}{dV_G} \quad (2)$$

where $L$ is the device channel length between the source and the drain and $C_t$ is the gate capacitance per unit length of the CNT. $C_t$ can be calculated from

$$C_t = \frac{2\pi\varepsilon_{ox}}{\ln(4t_{ox}/W)} \quad (3)$$

where $\varepsilon_{ox}$ is the effective dielectric constant of $SiO_2$ (3.9 $\varepsilon_o$), $t_{ox}$ is the oxide thickness (300 nm), and $W$ is the diameter of the CNT measured by AFM. The mobility determines how fast the device switches and limits the speed of the device. In Figure 1d, the peak mobility of the device is 3546 $cm^2/(V\ s)$. The conductance, the transconductance, and the mobility of device 1 are in the same order of magnitude as those of the highly performing CVD-grown CNT devices reported in ref 18 and ref 19. A second device (device 2) of an isolated FHP CNT with a diameter of 1.3 nm (AFM image and its height measurements in the supporting materials), shown in Figure 2a, also exhibited high mobility, conductance, and transconductance. In particular, it had an on/off ratio as high as $10^6$, as shown in Figure 2b.

Device 3 was fabricated using PtRhRe CNTs, and the SEM image is shown in Figure 3a. This device was the best performing semiconductor among the PtRhRe CNT devices examined. Its transfer characteristic is illustrated in Figure 3b. The device has an on-state conductance of 0.39 μS, a transconductance of 0.14 μS, a mobility of 52 $cm^2/(V\ s)$ and an on/off ratio of approximately 10. These values are considerably lower than those of devices 1 and 2, but are similar to previously reported values in the majority of solution-processed devices. Table 1 compares the parameters of the three devices presented in Figures 1−3 with the high-performing solution processed devices fabricated by Stokes *et al.*[12] as a

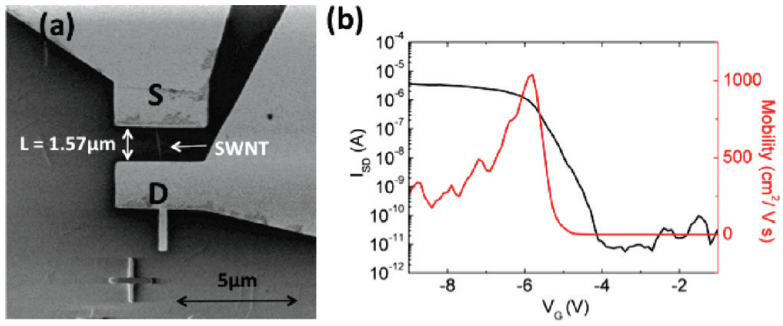


**Figure 2. Characterization of a second FHP CNT (device 2). (a) SEM image of the device 2 showing its channel length to be 1.57 μm; (b) transfer characteristics of device 2 showing the dependence of $I_{SD}$ and the mobility on $V_G$, when $V_{SD}$ = 1 V.**

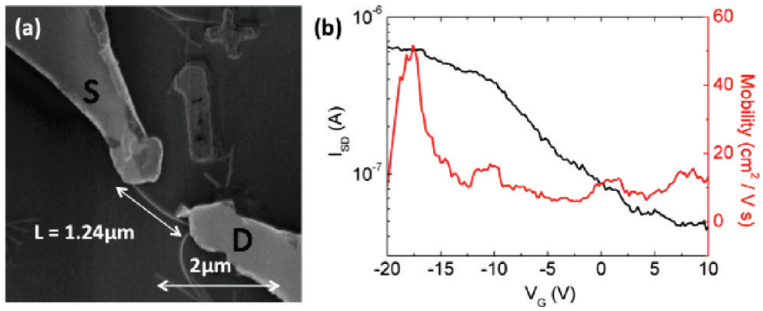


**Figure 3. Characterization of a PtRhRe CNT (device 3). (a) SEM image of the device 3 showing its channel length to be 1.24 μm; (b) transfer characteristics of device 3 showing the dependence of $I_{SD}$ and the mobility on $V_G$, when $V_{SD}$ = 1 V.**

reference. Compared to the reference device, device 1 fabricated in this work demonstrates higher mobility, conductance, and transconductance with a similar on/off ratio (close to $10^4$), while device 2 exhibits a higher on/off ratio of $10^6$.

To understand why the FHP CNTs exhibit such outstanding electrical transport properties, we characterized both the FHP and PtRhRe CNTs in terms of their cleanliness, catalyst content, amorphous carbon surface coverage, and defect content. This enables structure−property correlations to be elucidated. HRTEM images of the two types of CNTs dispersed on lacey TEM grids are shown in Figure 4. At low magnification, the catalyst particles were hardly seen, even in a very dense sample of the FHP CNTs, shown in Figure 4a. In contrast, the catalyst particles could be observed over the dilute bundles of PtRhRe CNTs, shown in Figure 4b. Raman spectroscopy and X-ray photoelectron spectroscopy have been previously used to show that a reaction between chlorine or hydrogen chloride and catalyst particles such as iron can occur and result in iron chloride dopants during sonication in 1,2-DCE and other chlorinated solvents.[20] In our case the catalyst particles may also react with chlorine or hydrogen chloride in 1,2-DCE during the sonication and cause doping in the PtRhRe CNTs. The dopants may act as charged impurities to scatter charge carriers and reduce the conductance and the mobility of the CNT devices.[6]

The structure of several FHP CNTs is resolved at a higher magnification in Figure 4c. Compared to the PtRhRe CNTs in Figure 4d, significantly less amorphous carbon was observed on the surface of the FHP CNTs. This amorphous carbon may affect the transport properties of the PtRhRe CNTs by creating a conduction barrier at the interface between the nanotube and the metal electrode. It may also lead to electrostatic potential fluctuations along the CNT channel, causing long-range disorder, which is especially important for semiconducting CNTs.[21] The potential fluctuations can break the CNT into a series of electronic puddles resulting in charge carriers hopping between the puddles.[21,22] This disorder could degrade the transport properties of the PtRhRe CNTs.

Figure 4 panels e and f show atomic-resolution HRTEM images of an isolated FHP SWNT and an isolated FHP DWNT, respectively. They are both clean and defect-free throughout this region. The appearance of DWNTs in the FHP CNT samples provides another possibility that the high mobility of the FHP devices may be due to the shielding of the inner shell of the tube from the outer shell during processing. However, extensive HRTEM analysis revealed that the majority of FHP CNTs with diameters 1.5 nm or less were primarily SWNTs, with the DWNTs typically having larger diameters. Isolated PtRhRe CNTs were harder to find and they were either covered with amorphous carbon or residuals, as shown in Figure 4g.

Raman spectra were also taken for devices 1 and 3 with a laser excitation of 532 nm. No D band peak was observed from device 1, as shown in Figure 5a, indicating that this CNT is relatively free from defects. The D band is attributed to defects such as impurities, amorphous carbon, or missing atoms in CNTs.[23] The CNT in device 3, shows a small D band in Figure 5b, possibly induced by the microwave digestion in aqua-regia or by impurities formed during the sonication in 1,2-DCE as discussed in the Methods section. These defects could cause the charge carriers to be scattered with a large momentum transfer[21] and reduce the transport performance of the PtRhRe CNT device. In addition, the inset graph in Figure 5b shows that the $G^+$ and the $G^-$ band peaks fit very well with a Lorentzian profile, which also indicates that CNT is semiconducting.[23] This agrees well with the transport measurement.

**TABLE 1. Summary of the Transport Properties of Our Devices and a Reference Device Fabricated by Stokes *et al.*[12]**

| device | diameter (nm) | on/off ratio | mobility ($cm^2/(V\ s)$) | $G_{on}$ (μS) | $g_m$ (μS) |
|---|---|---|---|---|---|
| ref 11 | 1.7 | $10^3-10^4$ | 1380 | 6.0 | 0.45 |
| 1 (FHP CNT) | 1.3 ± 0.1 | $10^3-10^4$ | 3546 | 9.35 | 4.22 |
| 2 (FHP CNT) | 1.5 ± 0.1 | $10^6$ | 1040 | 4.25 | 2.11 |
| 3 (PtRhRe CNT) | 2.0 ± 0.1 | ~10 | 52 | 0.39 | 0.14 |

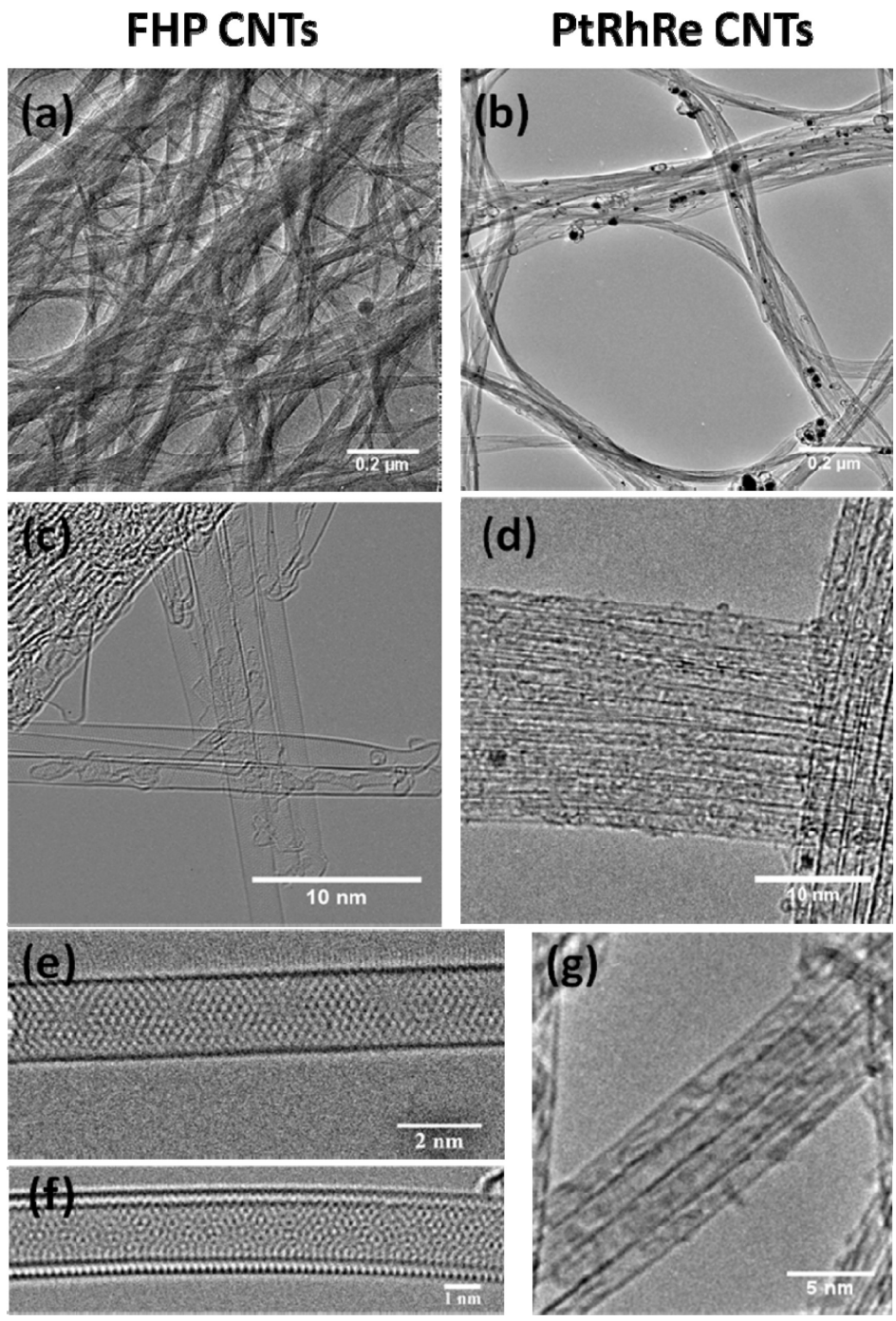


**Figure 4. TEM characterization of the FHP and the PtRhRe CNTs. Low-magnification TEM images of (a) the FHP CNTs and (b) the PtRhRe CNTs. Medium-magnification TEM images of (c) some FHP CNTs and (d) some PtRhRe CNTs. HRTEM images of (e) an FHP SWNT, (f) isolated FHP DWNT, and (g) small bundles of PtRhRe CNTs .**

By performing HRTEM and Raman spectroscopy on the two types of CNTs, we can correlate the structural and electrical properties. We find that the high-performing FHP CNT devices are free from defects, catalyst particles, and surface contamination. This is attributed to the high-temperature vacuum annealing the CNTs have undergone, combined with the use of 1,2-DCE as the solvent for dispersion. Sonicating CNTs in 1,2-DCE to disperse them does not leave behind any residue on the CNTs once they are dry, provided the CNT sample is of high purity to begin with, as shown by HRTEM. These results show that solution processing can be used to obtain clean and defect-free CNTs in high-performance field effect transistors. Generally, devices made with CNTs grown directly on substrates by CVD perform better than solution processed CNTs, as the CVD CNTs are not doped from catalyst particles during processing,

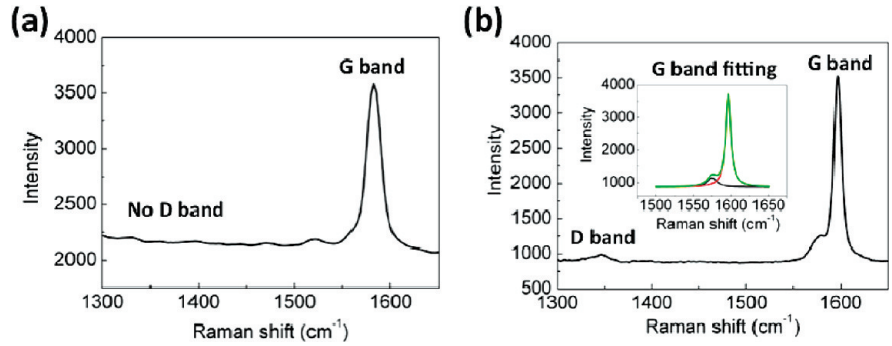


**Figure 5. Raman spectra for CNTs at 532 nm laser excitation: (a) G band and D band for FHP CNT in device 1; (b) G band and D band for PtRhRe CNT in device 3. The inset shows the fit of the $G^+$ and $G^-$ band by two Lorentzian profiles.**

are not exposed to harsh acids for purification, contain less amorphous carbon,[24] and are also less likely to have defects induced from sonication.[13] However, our work shows that by careful control of CNTs structure and cleanliness, solution processed CNTs can also exhibit high electrical performance.

## METHODS

**Types and Processing of CNTs.** We use two types of CNTs in devices. The first type were CNTs (FHP CNTs) generously provided by Meijo Nano Carbon Co., Ltd. They were synthesized by the arc-discharge method[25] and had diameters ranging from 1.2 up to 2.5 nm. The FHP CNTs contain predominantly single-walled carbon nanotubes (SWNTs) with a fraction of double-walled carbon nanotubes (DWNTs) and triple-walled carbon nanotubes (TWNTs). The FHP CNTs were subject to annealing at high temperatures (~1200 °C) under vacuum at a pressure of $10^{-6}$ mbar. At this temperature and pressure the metal catalyst particles vaporize and are removed from the sample under continuous dynamic vacuum pumping.[26] This also improved the quality of the CNTs by reducing the number of defects, possibly through a self-healing mechanisms. The second type of CNTs were SWNTs synthesized according to a previously reported method by laser ablation using nonmagnetic catalysts such as plantium (Pt), rhodium (Rh), and rhenium (Re) and had diameters ranging between 1.4 and 1.6 nm.[27] This type of CNTs is referred to as PtRhRe CNTs. They were purified by annealing in air and then using microwave digestion in aqua-regia.[28]

**Device Fabrication.** In all cases, the CNTs were sonicated in 1,2-dichloroethane (1,2-DCE) for 30 min for dispersion[29] and then spin coated onto silicon substrates with 300 nm thick oxide surface at 2000 rpm for 60 s. After the spin coating, CNT devices were fabricated using electron beam lithography (EBL) methods (JEOL JBX-5500FS). The drain and the source electrodes were Au/Cr with the thickness of 40 nm/10 nm. The highly doped silicon substrate was used as a back gate electrode. Atomic force microscopy (AFM) in noncontact mode was used to measure the diameters of CNTs (Park Scientific CP-II). Scanning electron microscopy (SEM) (Carl Zeiss Nanovision) was used to image the devices at a low accelerating voltage of 1 kV to give clear images of CNTs on the oxide surface.[30]

**Characterization of CNTs.** The transport properties of the devices without any postdeposition annealing processes were measured at room temperature in air using a custom-built probe station. After the transport measurements, Raman spectroscopy (Horiba Jobin Yvon LabRam Aramis) was used to determine the defects of the CNTs in the device. The dispersed CNTs were also deposited onto TEM grids for characterization. Conventional high-resolution transmission electron microscopy (HRTEM) was performed using a JEOL 4000 at the accelerating voltage of 80 kV, while atomic-resolution HRTEM was performed using Oxford's JEOL 2200MCO equipped with both probe and image correctors at 80 kV.[31]

*Acknowledgment.* J.H.W. thanks the Glasstone Fund and Brasenose College, Oxford for support. G.A.D.B. thanks the EPSRC for support (GR/S15808/01). M.H.R. thanks the EU (ECEMP) and the Freistaat Sachsen. F.S acknowledges support from the Alexander von Humboldt foundation and the BMBF. We thank A. Crossley, S. Myhra, C. Johnston, R. Chakalova, R. George and Y. Xing for assistance.

*Supporting Information Available:* AFM charaterization to determine the error in the CNT height measurements, and the method to get Raman signal for isolated CNT; statistics of transport performance for the semiconducting devices. This material is available free of charge *via* the Internet at http://pubs.acs.org.

## REFERENCES AND NOTES

1. Martel, R.; Schmidt, T.; Shea, H. R.; Hertel, T.; Avouris, P. Single- and Multiwall Carbon Nanotube Field-Effect Transistors. *Appl. Phys. Lett.* **1998**, *73*, 2447–2449.
2. Tans, S. J.; Verschueren, A. R. M.; Dekker, C. Room-Temperature Transistor Based on a Single Carbon Nanotube. *Nature* **1998**, *393*, 49–52.
3. Kong, J.; Franklin, N. R.; Zhou, C.; Chapline, M. G.; Peng, S.; Cho, K.; Dai, H. Nanotube Molecular Wires as Chemical Sensors. *Science* **2000**, *287*, 622–625.
4. Fuhrer, M. S.; Kim, B. M.; Dürkop, T.; Brintlinger, T. High-Mobility Nanotube Transistor Memory. *Nano Lett.* **2002**, *2*, 755–759.
5. Hellstrom, S. L.; Lee, H. W.; Bao, Z. Polymer-Assisted Direct Deposition of Uniform Carbon Nanotube Bundle Networks for High-Performance Transparent Electrodes. *ACS Nano* **2009**, *3*, 1423–1430.
6. Dürkop, T.; Getty, S. A.; Cobas, E.; Fuhrer, M. S. Extraordinary Mobility in Semiconducting Carbon Nanotubes. *Nano Lett.* **2003**, *4*, 35–39.
7. Javey, A.; Guo, J.; Wang, Q.; Lundstrom, M.; Dai, H. Ballistic Carbon Nanotube Field-Effect Transistors. *Nature* **2003**, *424*, 654–657.
8. Weitz, R. T.; Zsehiesehang, U.; Forment-Aliaga, A.; Kälblein, D.; Burghard, M.; Kern, K.; Klauk, H. Highly Reliable Carbon Nanotube Transistors with Patterned Gates and Molecular Gate Dielectric. *Nano Lett.* **2009**, *9*, 1335–1340.
9. Roberts, M. E.; LeMieux, M. C.; Sokolov, A. N.; Bao, Z. Self-Sorted Nanotube Networks on Polymer Dielectrics for Low-Voltage Thin-Film Transistors. *Nano Lett.* **2009**, *9*, 2526–2531.
10. Arnold, M. S.; Green, A. A.; Hulvat, J. F.; Stupp, S. I.; Hersam, M. C. Sorting Carbon Nanotubes by Electronic Structure Using Density Differentiation. *Nat. Nanotechnol.* **2006**, *1*, 60–65.
11. LeMieux, M. C.; Roberts, M.; Barman, S.; Yong, W. J.; Jong, M. K.; Bao, Z. Self-Sorted, Aligned Nanotube Networks for Thin-Film Transistors. *Science* **2008**, *321*, 101–104.

12. Stokes, P.; Khondaker, S. I. High Quality Solution Processed Carbon Nanotube Transistors Assembled by Dielectrophoresis. *Appl. Phys. Lett.* **2010**, 96.
13. Hennrich, F.; Krupke, R.; Arnold, K.; Rojas Stütz, J. A.; Lebedkin, S.; Koch, T.; Schimmel, T.; Kappes, M. M. The Mechanism of Cavitation-Induced Scission of Single-Walled Carbon Nanotubes. *J. Phys. Chem. B* **2007**, *111*, 1932–1937.
14. Vijayaraghavan, A.; Blatt, S.; Weissenberger, D.; Oron-Carl, M.; Hennrich, F.; Gerthsen, D.; Hahn, H.; Krupke, R. Ultra-Large-Scale Directed Assembly of Single-Walled Carbon Nanotube Devices. *Nano Lett.* **2007**, *7*, 1556–1560.
15. Kim, W.-J.; Lee, C. Y.; O'brien, K. P.; Plombon, J. J.; Blackwell, J. M.; Strano, M. S. Connecting Single Molecule Electrical Measurements to Ensemble Spectroscopic Properties for Quantification of Single-Walled Carbon Nanotube Separation. *J. Am. Chem. Soc.* **2009**, *131*, 3128–3129.
16. Wang, W. M.; LeMieux, M. C.; Selvarasah, S.; Dokmeci, M. R.; Bao, Z. Dip-Pen Nanolithography of Electrical Contacts to Single-Walled Carbon Nanotubes. *ACS Nano* **2009**, *3*, 3543–3551.
17. Lee, T. C.; Tsui, B. Y.; Tzeng, P. J.; Wang, C. C.; Tsai, M. J. A Process for High Yield and High-Performance Carbon Nanotube Field Effect Transistors. *Microelectron. Reliab.* **2010**, *50*, 666–669.
18. Javey, A.; Kim, H.; Brink, M.; Wang, Q.; Ural, A.; Guo, J.; McIntyre, P.; McEuen, P.; Lundstrom, M.; Dai, H. High-κ Dielectrics for Advanced Carbon-Nanotube Transistors and Logic Gates. *Nat. Mater.* **2002**, *1*, 241–246.
19. Zhang, Z.; Wang, S.; Ding, L.; Liang, X.; Pei, T.; Shen, J.; Xu, H.; Chen, Q.; Cui, R.; Li, Y.; *et al*. Self-Aligned Ballistic n-Type Single-Walled Carbon Nanotube Field-Effect Transistors with Adjustable Threshold Voltage. *Nano Lett.* **2008**, *8*, 3696–3701.
20. Moonoosawmy, K. R.; Kruse, P. To Dope or Not to Dope: The Effect of Sonicating Single-Wall Carbon Nanotubes in Common Laboratory Solvents on Their Electronic Structure. *J. Am. Chem. Soc.* **2008**, *130*, 13417–13424.
21. Ado Jorio, M. S. D., Dresselhaus, G. *Carbon Nanotubes: Advanced Topics in the Synthesis, Structure, Properties and Applications*; Springer: New York, 2008.
22. Gao, B.; Glattli, D. C.; Plaçais, B.; Bachtold, A. Co-tunneling and One-Dimensional Localization in Individual Disordered Single-Wall Carbon Nanotubes: Temperature Dependence of the Intrinsic Resistance. *Phys.Rev. B* **2006**, *74*, 085410.
23. Dresselhaus, M. S.; Dresselhaus, G.; Saito, R.; Jorio, A. Raman Spectroscopy of Carbon Nanotubes. *Phys. Rep.* **2005**, *409*, 47–99.
24. Chikkannanavar, S. B.; Luzzi, D. E.; Paulson, S.; Johnson, A. T. Synthesis of Peapods Using Substrate-Grown SWNTs and DWNTs: An Enabling Step Toward Peapod Devices. *Nano Lett.* **2004**, *5*, 151–155.
25. Zhao, X.; Inoue, S.; Jinno, M.; Suzuki, T.; Ando, Y. Macroscopic Oriented Web of Single-Wall Carbon Nanotubes. *Chem. Phys. Lett.* **2003**, *373*, 266–271.
26. Kitaura, R.; Ogawa, D.; Kobayashi, K.; Saito, T.; Ohshima, S.; Nakamura, T.; Yoshikawa, H.; Awaga, K.; Shinohara, H. High-Yield Synthesis and Characterization of The Structural and Magnetic Properties of Crystalline $ErCl_3$ Nanowires in Single-Walled Carbon Nanotube Templates. *Nano Res.* **2008**, *1*, 152–157.
27. Rümmeli, M. H.; Löffler, M.; Kramberger, C.; Simon, F.; Fülöp, F.; Jost, O.; Schönfelder, R.; Grüneis, A.; Gemming, T.; Pompe, W.; *et al*. Isotope-Engineered Single-Wall Carbon Nanotubes; A Key Material for Magnetic Studies. *J. Phys. Chem. C* **2007**, *111*, 4094–4098.
28. Schönfelder, R.; Rümmeli, M. H.; Gruner, W.; Löffler, M.; Acker, J.; Hoffmann, V.; Gemming, T.; Büchner, B.; Pichler, T. Purification-Induced Sidewall Functionalization of Magnetically Pure Single-Walled Carbon Nanotubes. *Nanotechnology* **2007**, 18.
29. Kim, K. K.; Bae, D. J.; Yang, C. M.; An, K. H.; Lee, J. Y.; Lee, Y. H. Nanodispersion of Single-Walled Carbon Nanotubes Using Dichloroethane. *J. Nanosci. Nanotechnol.* **2005**, *5*, 1055–1059.
30. Homma, Y.; Suzuki, S.; Kobayashi, Y.; Nagase, M.; Takagi, D. Mechanism of Bright Selective Imaging of Single-Walled Carbon Nanotubes on Insulators by Scanning Electron Microscopy. *Appl. Phys. Lett.* **2004**, *84*, 1750–1752.
31. Warner, J. H.; Schaffel, F.; Zhong, G.; Rummeli, M. H.; Buchner, B.; Robertson, J.; Briggs, G. A. D. Investigating the Diameter-Dependent Stability of Single-Walled Carbon Nanotubes. *ACS Nano* **2009**, *3*, 1557–1563.